IMaging-based CUSTOMised EYE diagnostics

Project ID: 779960

Funded under: H2020-EU.2.1.1. - INDUSTRIAL LEADERSHIP - Leadership in enabling and industrial technologies - Information and Communication Technologies (ICT)

Deliverable D4.5

Fabricated dynamic OCT prototype

This project has received funding from the *European Union's Horizon 2020 research and innovation programme* under grant agreement No 779960.

Document control information	
Title	D4.5 Fabricated dynamic OCT prototype
Contributing partners	IPC PAS, CSIS, Liverpool
Type	Demonstrator
Dissemination level	❒ **CO** Confidential, only for members of the consortium (including the Commission Services) ❒ **RE** Restricted to a group specified by the consortium (including the Commission Services) ❒ **PP** Restricted to other programme participants (including the Commission Services) ☒ **PU** Public
Status	❒ Draft ☒ WP Manager accepted ☒Co-ordinator accepted
Due date	30.11.2021
Delivery date	11.01.2022
Action requested	❒ to be revised by Partners involved in the preparation of the deliverable ❒ to be reviewed by applicable IMCUSTOMEYE Partners ❒ for approval of the WP Manager ❒ for approval of the Project Coordinator

Revision history			
Version	**Date**	**Author**	**Comment**
1.0	15.11.2021	Karol Karnowski	First draft
2.0	5.12.2021	Karol Karnowski	Final draft
3.0	8.12.2021	Maciej Wojtkowski	Approved on IPC PAS side
4.0	16.12.2021	Judith Birkenfeld	Minor edits, first approval from CSIC side
4.1	04.01.2021	Susana Marcos	Final approval from CSIC

This project has received funding from the *European Union's Horizon 2020 research and innovation programme* under grant agreement No 779960.

Table of contents

This project has received funding from the *European Union's Horizon 2020 research and innovation programme* under grant agreement No 779960.

1 Summary

This report relates to **the ImMIDscreener** - the physical compact device. The device was designed, assembled, and optimized for planned clinical measurements on a group of healthy and diseased corneas.

The assembly and optimization part of this work was performed at the Laboratories of Physical Optics and Biophotonics Group (POB) which is a part of the Institute of Physical Chemistry PAS (IPC PAS). Recently, POB became a part of the International Center of Translational Eye Research (ICTER) – a new research center that is a part of IPC PAS.

POB researchers worked in close collaboration with Madrid partners (Visual Optics and Biophotonics Lab from the Spanish National Research Council), who provide useful feedback from their studies on **ImTOPscanner** [1]. The conceptual assumptions for the **ImMIDscreener** device were based on FEM simulations performed by the Liverpool partners (Ocular Biomechanics Group from the University of Liverpool) and first results from the ImTOPScanner.

The concept of **imMIDscreener** grew from the fruitful IMCUSTOMEYE consortium discussions and was strengthened by FEM simulation results performed by Liverpool partners. Several corneal models with various central corneal thicknesses (CCT) and material stiffness were analyzed. Additionally, keratoconus eyes with various cone centers and radii were included in the analysis. In total, 50 heathy and 600 keratoconus models were used.

The spot distribution that was estimated to produce the optimal deformation asymmetry quantification was: 9-spot setup with a central spot to measure CCT and apex deformation, and 8 spots along a ~1.1 mm radius circumference (Fig.1).

The FEM modeling revealed that with only 9 points at which deformation is measured, one can estimate IOP and material stiffness. Also, for pathologies such as keratoconus, it is possible to identify the cone location and the mechanical weakening within the cone.

2 Introduction

Small footprint is a project-goal for the ImMIDscreener device. Although fundamental tradeoffs regarding imaging optics have prevented from reducing size to allow handheld operation, we have delivered a platform with a footprint similar to conventional equipment ophthalmology clinics with an imaging head that can be mounted to manual joystick operated base and a head/chin rest. Fig. 1 shows a rendering of an artistic rendering of the prototype, which has now been fabricated (except for the cover, which will be 3D printed and delivered in the next few weeks) and ready to be tested in the clinic.

This project has received funding from the *European Union's Horizon 2020 research and innovation programme* under grant agreement No 779960.

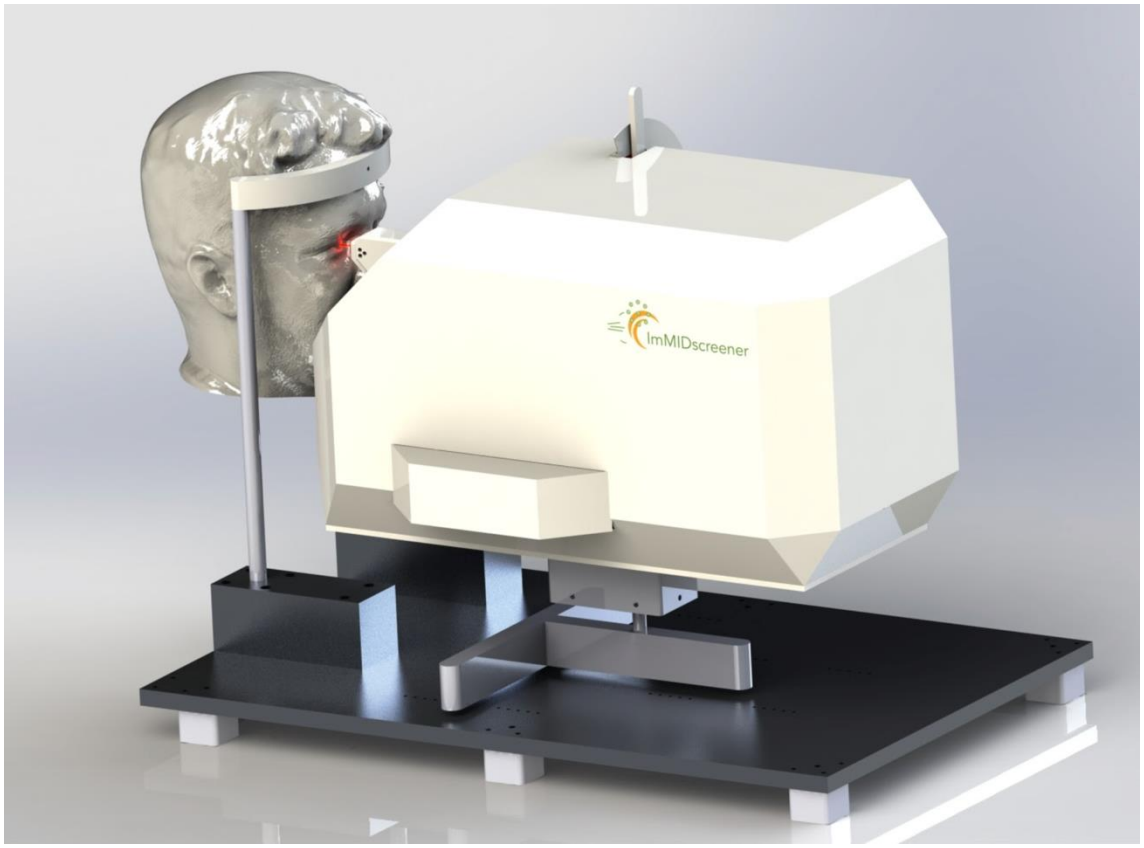

Fig.1 Artistic vision (3D rendering) of the ImMIDscreener clinical prototype.

3 ImMIDscreener

State-of-the-art OCT technology (high acquisition rates and appropriate swept source coherence properties) has allowed handling simultaneous acquisitions of 9-spot corneal locations. For simultaneous multi-spot measurements, a space division, depth-encoded multiplexing method is used [2]. The specs have been allowed by the use of light source with narrow instantaneous linewidth, and n appropriate bandwidth acquisition board for signal sampling. This has allowed different imaging spots to be recorded in the same OCT image, but at different different depths, enabled by a fine adjustment of every channel pathlengths.

3.1 Interferometer and light source

As a light source, we use a commercial grade swept laser from Thorlabs (SL131090). The laser operates at 1300 nm central wavelength with ~100 nm wavelength tuning range and 100 kHz repetition rate.

The laser unit provides synchronization outputs: central wavelength-based sweep trigger and a clock signal for even sampling in wavenumber domain (k-clock). The k-clock when used as an external clock source for digitizer will provide 11 mm OCT imaging depth range.

The fiber-based interferometer is a key component of every modern OCT system. Here we utilized a modified Mach-Zehnder interferometer (Fig. 2). The

This project has received funding from the *European Union's Horizon 2020 research and innovation programme* under grant agreement No 779960.

light from the source is split on a fiber coupler (75/25) and delivered via optical circulators to sample (75%) and reference (25%) arm. In the reference arm, the light is reflected from the reference mirror. The light in the sample arm is transmitted to imaging optics using optical coupler with β/(1-β) splitting ratio (β chosen to be 90%).

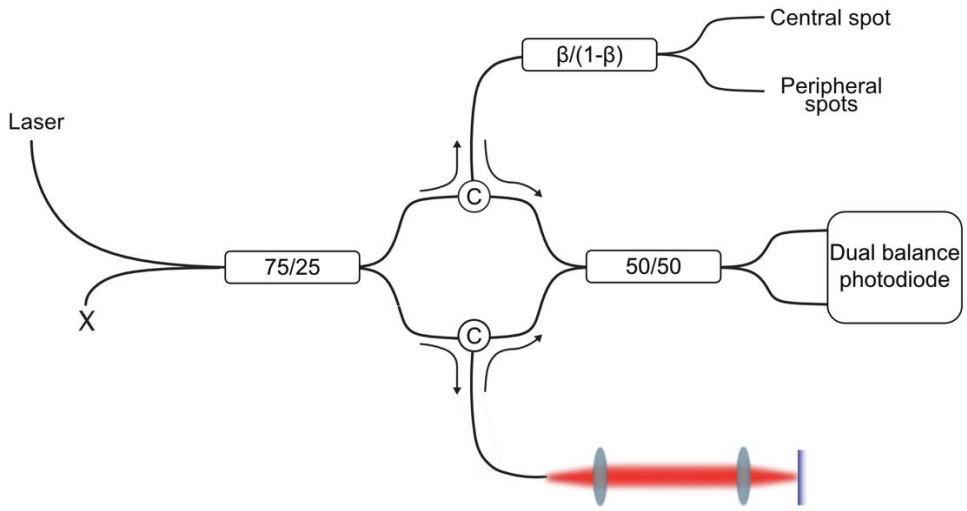

Fig. 2 Configuration of interferometric module of multi-spot air-puff system.

The splitting factor β defines the illumination powers as well as collection efficiency for central spot and peripheral spots. Light on "peripheral" path of β/(1-β) coupler is split to 8 spots with 1x8 fiber coupler providing 12.5% light delivery and collection efficiency (Fig. 3A).

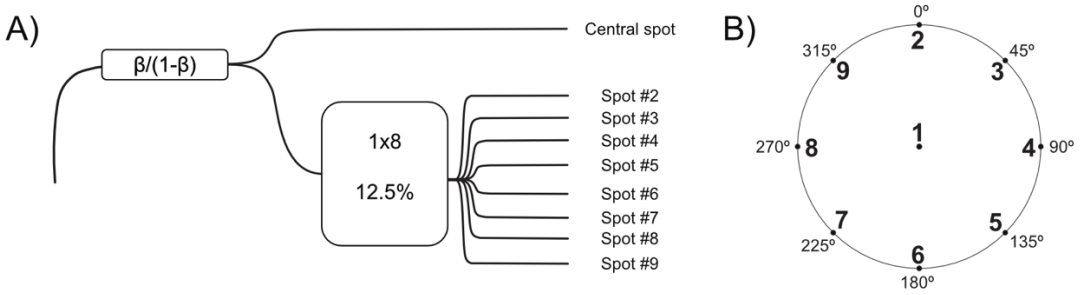

Fig. 3 A) Detailed fiber configuration of imMIDscreener sample arm. B) Schematic of multi-spot spatial arrangement.

Summary of illumination powers achieved for optical coupler with β =90% is presented in Table 1. The 90%/10% coupler ratio was chosen as optimal to keep the per-channel illumination at closest levels possible without sacrificing imaging quality for central channel.

Table 1 Summary of illumination optical power at output channels of the device.

Channel number (see Fig. 3 B)	Power at the sample [mw]
1 (central)	1.6
2	0.96

This project has received funding from the *European Union's Horizon 2020 research and innovation programme* under grant agreement No 779960.

3	0.95
4	1.05
5	1.07
6	1.02
7	1.09
8	1
9	1.03
Total power for 9-spots	9.77

Since we must split the power of the light from the source between 9 channels in the sample arm and the reference arm, we added an optical booster amplifier stage. Interferometer, reference arm, booster optical amplifier and dual balance detector were carefully organized to fit halt of the 19" rack case (Fig. 4).

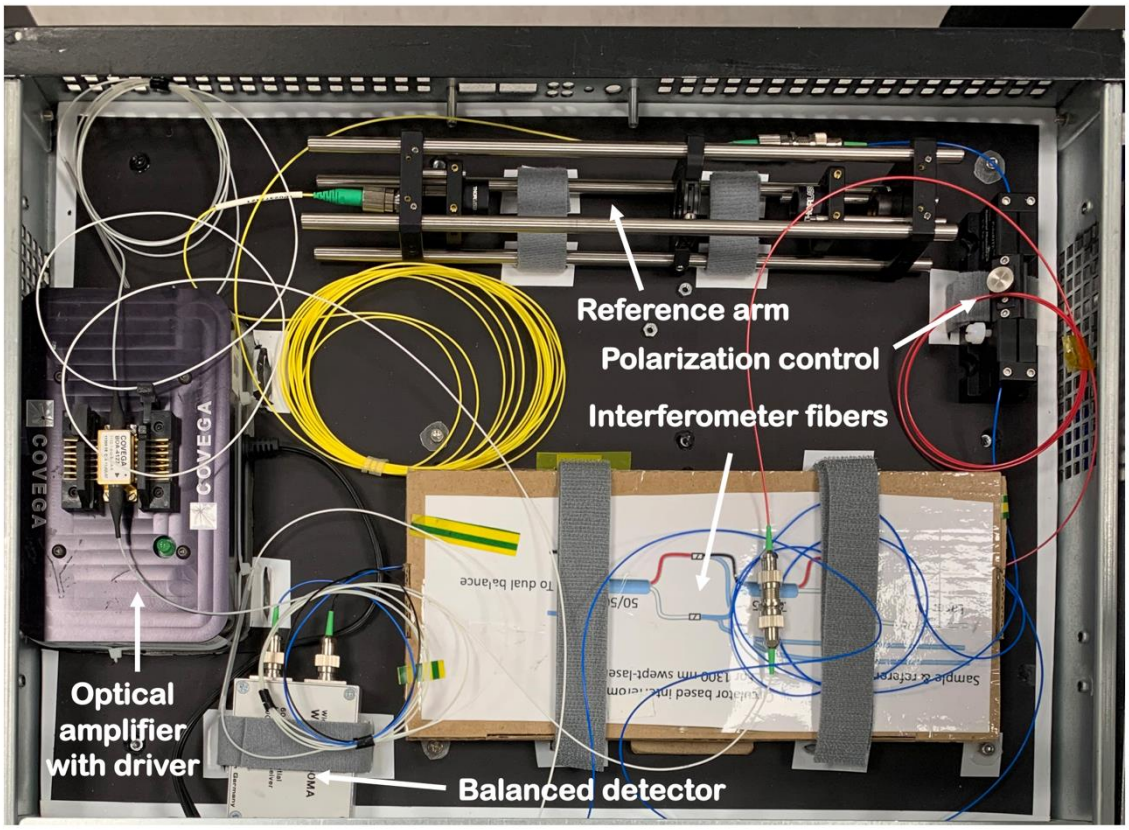

Fig. 4 Compact organization of some optical components in 19" rack case.

3.2 Imaging head

As a result of detailed FEM simulations performed by the IMCUSTOMEYE partners from the University of Liverpool the optimal spot number and spatial distribution was selected. The central spot is aimed at estimating apex corneal deformations and cornea thickness. The remaining peripheral points (2-9 on Fig. 3B) are arranged circumferentially at 1.1 mm distance from the central point.

For practical reasons we decided to keep central spot and peripheral spot optics separated. First, it enabled both beam scanning for the central spot and

This project has received funding from the *European Union's Horizon 2020 research and innovation programme* under grant agreement No 779960.

provided a cross-scan (horizontal and vertical) preview mode for patient alignment. Moreover, having 8 peripheral spots separated from central one we received freedom of spatial and temporal (pathlength) alignment.

3.2.1 Central spot

The scanning pattern of the central spot is realized using a pair of galvanometer scanners (with 5mm mirrors). The pattern is relayed to the imaging optics using 4f system consisting of two 300mm 2-inch lenses (Fig. 5). The decision of using 300mm lenses 4f system was dictated by the geometry constrains of 8-spot peripheral optics.

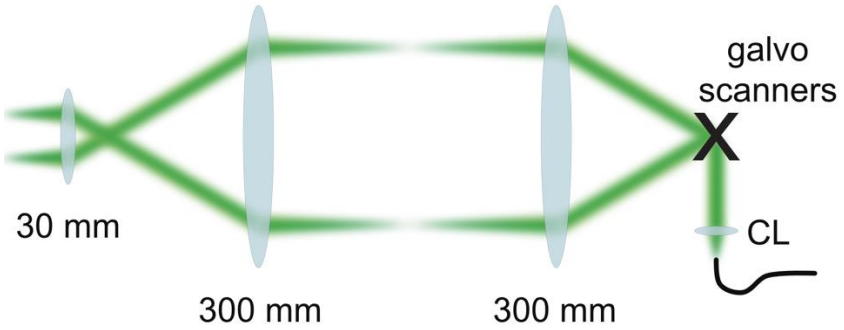

Fig. 5 Optical arrangement of the central spot with marginal beams of scanning pattern given in green color. CL – collimator lens package.

3.2.2 Peripheral spots

The central spot is combined with the remaining 8 spots using an array of 8 prism mirrors (yellow squares in the center of Fig. 6A). The corresponding beams for each of 8 peripheral spots are collimated first (CL on Fig. 6B) and then directed with a mirror onto the mirror array (we have here two degrees of freedom for alignment – kinematic mount for collimator and kinematic corner cube). Collimators are mounted on the rod system and their position along the beam axis can be aligned to tune the channel pathlength. By careful alignment, each of the 8 spot beams is made to intersect at the back focal plane of the imaging lens. As result (assuring right beam angles), the beam separation at the sample plane can be set as required. The separation is a function of the beam angle and the focal length of the imaging lens. The beam angle (compatible with the mirrors spacing and distance from the imaging lens) that minimized the impact of the mirror array on the scanned central beam (shadowing on the mirror array sharp edges) was set to 22.5^{o} (Fig. 6A green).

This project has received funding from the *European Union's Horizon 2020 research and innovation programme* under grant agreement No 779960.

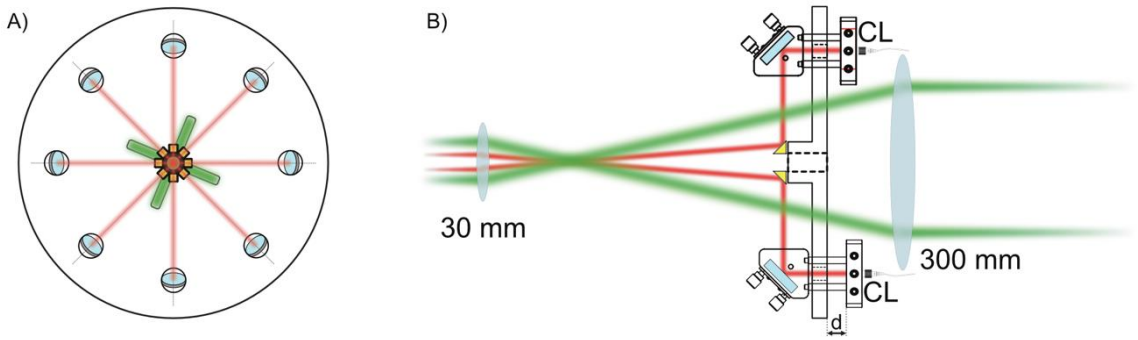

Fig. 6 The optical arrangement of the peripheral spots (red color) with marginal beams of scanning pattern added for a reference. A) front view with cross opening for preview mode central beam visible (green). 8-beams (red) are pointing on the mirror array in the central part to be reflected towards the imaging lens. B) Side view with showing for simplicity two out of 8 mirrors and central scanned beam. The configuration enables adjustment of the pathlength (d) for each of the 8 spots separately. CL – collimator lens package.

3.2.3 Merging of all 9 spots

To merge the optics associated to all 9-spots we carefully designed (Fig. 7A) and fabricated dedicated mounts and adapters. The path for 4f system (1200 mm in total) was broken 4 times and the beam was routed on such broken path horizontally and vertically. As a result, the length of this part was reduced by a factor of 2 and enabled assembly of reasonable compact clinical- grade imaging platform.

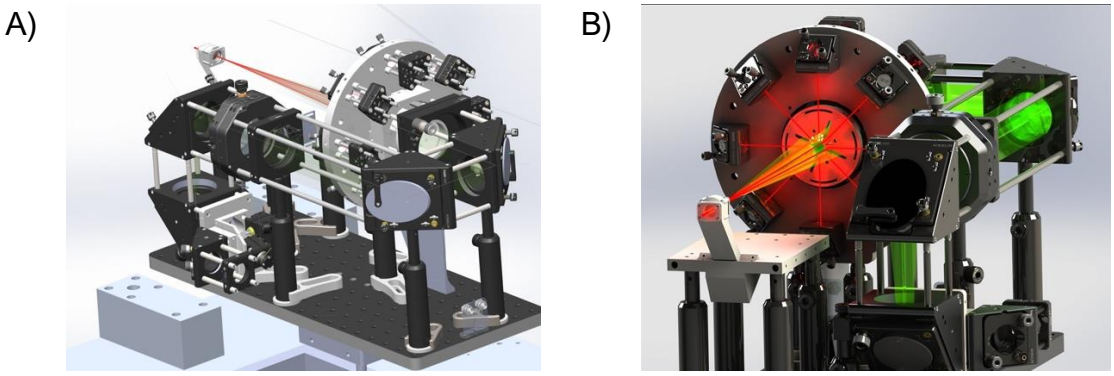

Fig. 7 A) 3D rendering of the imaging optics of the imMIDscreener prepared to be mounted on clinical grade joystick and chinrest platform. B) Different 3D rendering view with simulations of the 8 peripheral beams traveling through the system components.

A separate mount was created for 8-spot part of the system. It contains an array of collimator and corner cube mirror reflectors (Fig. 7B). In final ImMIDscreener device the mirror array is on joint mount module with one of 4f system lenses with an option of separate tilt alignment of mirror's array and the lens and adjustment of lens position along optical axis of the system (Fig. 7 A and B). The tilted cross-opening for central scanning spot is also visible on 3D rendering (Fig. 7B).

This project has received funding from the *European Union's Horizon 2020 research and innovation programme* under grant agreement No 779960.

3.3 Electronics

Electronics components include: DC power supply units (optical amplifier, air-puff, balanced detector, scanners driver), XY scanners driver, and Arduino-based unit for air-puff activation/synchronization. To facilitate handling and transportation we organized all those components into half of 19” rack case (Fig. 8).

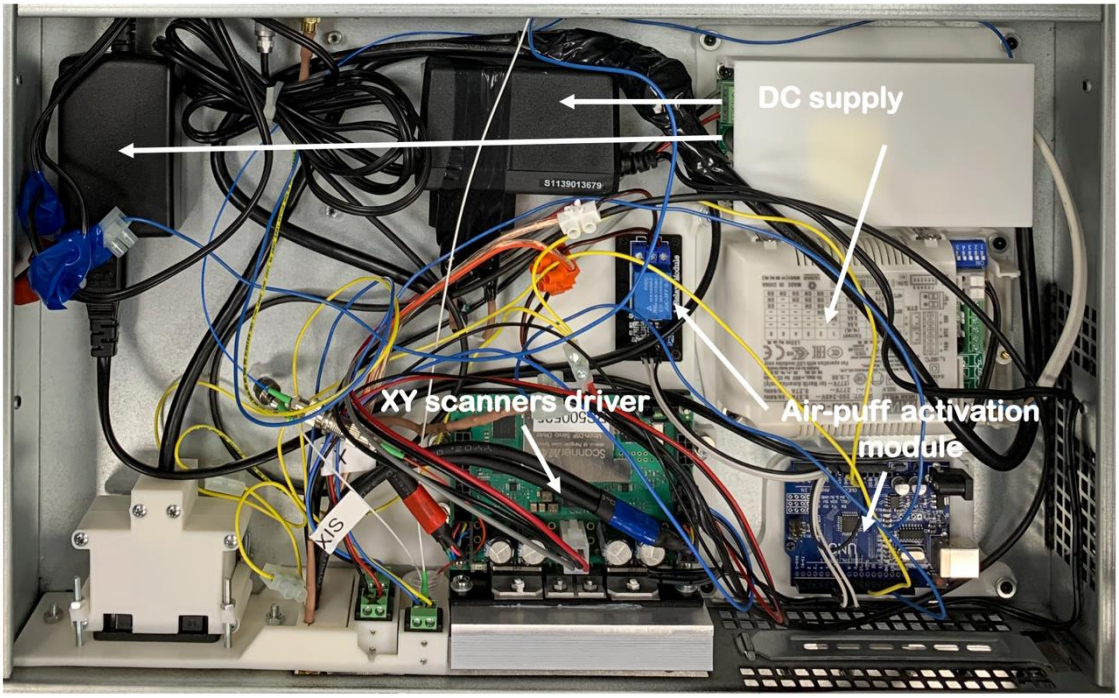

Fig. 8 Compact organization of some electrical components in 19” rack case.

3.4 Air-puff module

Air-puff module is an integral part of the ImMIDscreener device. The general approach for air-puff OCT measurements is to use a repurposed air-puff module from commercial devices such as the Nidek 2000 or Reichert Xpert Plus [3][4]. The limitation of such approach is that the rear window, through which the OCT beam/s enter/s the chamber is not AR coated. In Deliverable D2.1 we proposed to replace the rear window with the lens we are using for imaging (D.2.1 Fig. 1). We designed a new chamber (Fig. 9 A) and repurposed some key elements from a commercial Reichert Xpert Plus module (e.g., solenoid motor, piston). In our custom design the 30 mm focal length lens that is used for focusing of all 9 spots on the corneal surface (Fig. 9 B), was placed at the rear side of on the chamber optical axis. We added additional housing part (Fig. 9 C) to improve the stability and enable fine adjustments of the air-puff chamber head tilt.

This project has received funding from the *European Union’s Horizon 2020 research and innovation programme* under grant agreement No 779960.

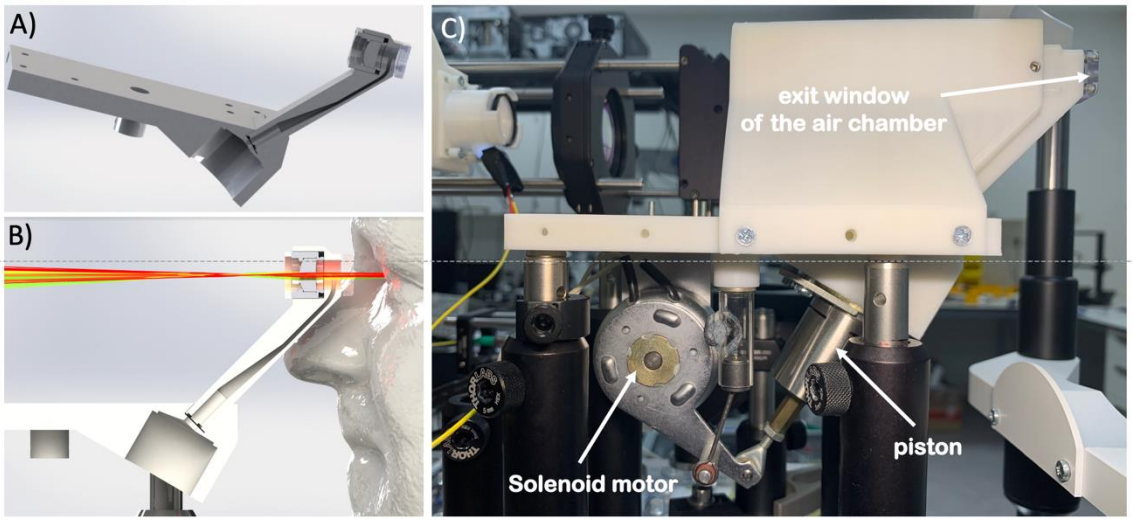

Fig. 9 A) 3D rendering of custom part of air-puff chamber, B) 3D rendering visualizing the head of the air-puff chamber aligned for measurement with peripheral (red) and central (green) beams added. C) A photography of assembled air-puff chamber with original parts from commercial device and additional housing.

3.5 Fixation target

To minimize the eye movements during the alignment procedure and ensure measurements along correct eye axis, we designed a prototype of binocular fixation target module (Fig. 10). 3D printed gears with laver enables fine adjustment of the fixation target position for both patient eyes according to the interpulipary distance.

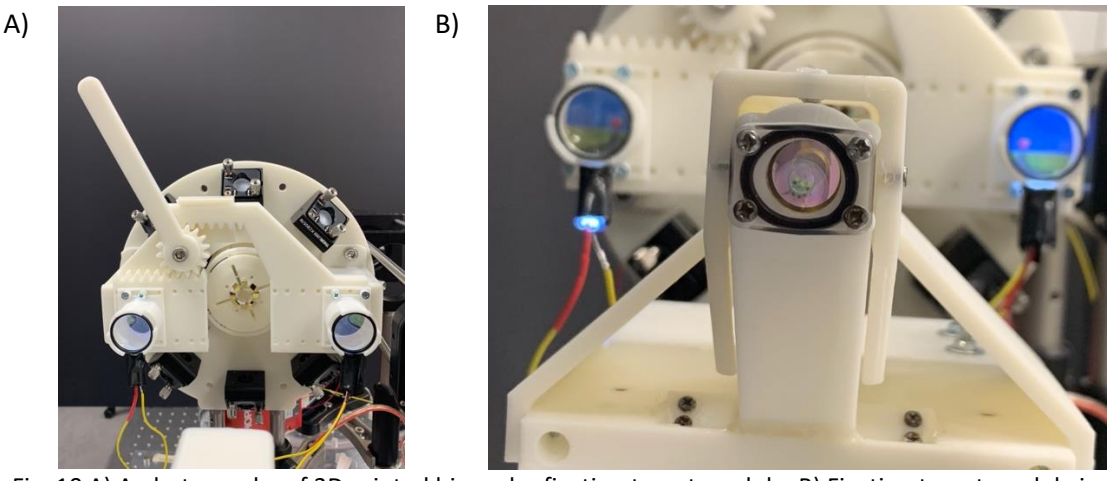

Fig. 10 A) A photography of 3D printed binocular fixation target module. B) Fixation target module in background of the air-puff chamber nozzle.

3.6 ImMIDscreener operation scheme

As mentioned earlier, to enable clinical measurements, the imaging module of the system was placed on a mobile platform manually controlled with a joystick (Fig. 11). The whole system, as in similar clinical systems of this type, is complemented by a chin/head rest component.

This project has received funding from the *European Union's Horizon 2020 research and innovation programme* under grant agreement No 779960.

A) 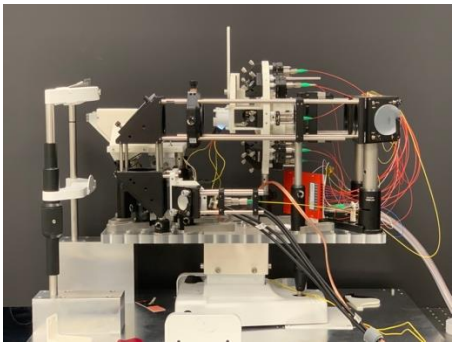 B) 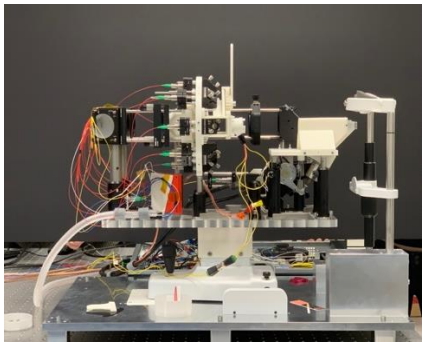

Fig. 11 A) and B) Side view photos of ImMIDscreener imaging head module mounted on clinical-grade moveable platform.

The alignment of the patient is possible thanks to the central spot scanning ability and a dedicated preview mode in developed, python-based acquisition software. Using horizontal and vertical preview cross-sectional images, the operator can easily align the position of air-puff nozzle and imaging optics to ensure deformation measurements aligned to the apex of the cornea.

The software continuously analyzes the preview images and when it confirms an optimal alignment (specular reflection appears on both cross sections) the scanning beam is centered, and the air pulse is activated. Simultaneously the raw data of the 9-spot corneal deformation are recorded. Immediately after the measurement, the operator can preview graphic file with the recorded deformation profiles (.png file format). In addition, the last preview images are saved as separate graphic file. This allows the operator to quickly assess whether the measurement was successful and repeat the measurement if necessary.

The software module for automatic segmentation of temporal deformation profile for each of 9-spot is under development. For now, the deformation asymmetries are assessed in mixed manual-automated mode using the Labview based software module.

4 Preliminary results

All ImMIDscreener device components described above enabled fine spatial adjustment of all 9 spots (Fig. 12A). The ability of fine tuning of the temporal offsets between channels (path-length adjustment) enabled simultaneous imaging of air-induced corneal deformation at all 9-spots as presented with the preliminary measurements on healthy volunteer in vivo (Fig. 12B).

A) 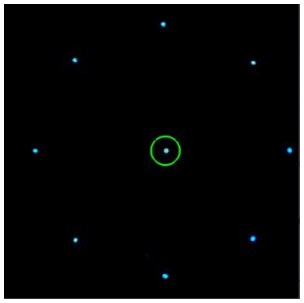 B) 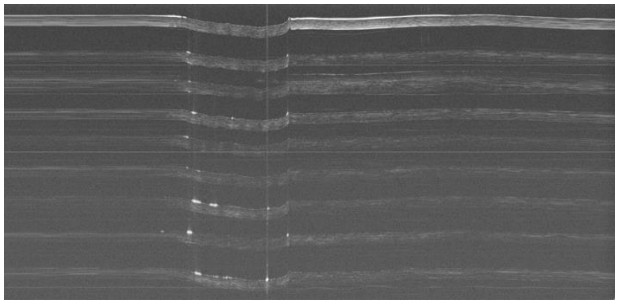

Fig. 12 A) Spatial distribution the 9 spots in the focal plane of the imaging beams. B) Exemplary result of in vivo human volunteer measurement with imMIDscreener system.

This project has received funding from the *European Union's Horizon 2020 research and innovation programme* under grant agreement No 779960.

5 Conclusions

In this document, we demonstrated the physical prototype of the ImMIDscreener device. The instrument, showcasting a similar footprint as many clinical ophthalmic devices is ready for the clinical measurements planned within the IMCUSTOMEYE project.

Some of key parameters of constructed ImMIDscreener device are given is Table below.

Table 1. Key parameters of ImMIDscreener protptype

Imaging module	
Number of measurements spots	9 (measured simultaneously)
Diameter of the 8 peripheral spots circle	2.2 mm
Temporal resolution	10 μs (for each spot simultaneously)
Axial resolution	13 μm
Axial imaging range	22 mm
Measurement	
Output files	Preview (png) Measurement (png, raw h5)
Deformation image size	5480 (time) x 2560 (depth) px (png) 5480 (time) x 5120* (depth) px (h5) * or higher power of 2
Electrical	
Voltage	240 VAC
Frequency	50-60 Hz
Dimensions (Platform only)	
Width	45 cm
Height	55 cm
Depth	75 cm

This project has received funding from the *European Union's Horizon 2020 research and innovation programme* under grant agreement No 779960.

6 References

[1] A. Curatolo *et al.*, "Multi-meridian corneal imaging of air-puff induced deformation for improved detection of biomechanical abnormalities," *Biomed. Opt. Express, Vol. 11, Issue 11, pp. 6337-6355*, vol. 11, no. 11, pp. 6337–6355, Nov. 2020, doi: 10.1364/BOE.402402.

[2] C. Fhou, A. Alex, J. Rasakanthan, and Y. Ma, "Space-division multiplexing optical coherence tomography," *Opt. Express, Vol. 21, Issue 16, pp. 19219-19227*, vol. 21, no. 16, pp. 19219–19227, Aug. 2013, doi: 10.1364/OE.21.019219.

[3] D. Alonso-Caneiro, K. Karnowski, B. Kaluzny, A. Kowalczyk, and M. Wojtkowski, "Assessment of corneal dynamics with high-speed swept source Optical Coherence Tomography combined with an air puff system," *Opt. Express*, vol. 19, no. 15, p. 14188, 2011.

[4] C. Dorronsoro, D. Pascual, P. Pérez-Merino, S. Kling, and S. Marcos, "Dynamic OCT measurement of corneal deformation by an air puff in normal and cross-linked corneas," *Biomed. Opt. Express, Vol. 3, Issue 3, pp. 473-487*, vol. 3, no. 3, pp. 473–487, Mar. 2012, doi: 10.1364/BOE.3.000473.

This project has received funding from the *European Union's Horizon 2020 research and innovation programme* under grant agreement No 779960.